Biointerface Research in Applied Chemistry
Open-Access Journal (ISSN: 2069-5837)

Article
Volume 13, Issue 4, 2023, 374
https://doi.org/10.33263/BRIAC134.374

Quantum Calculation, Docking, ADMET and Molecular Dynamics of Ketal and Non-ketal Forms of D-glucofuranose Against Bacteria, Black & White Fungus, and Triple-Negative Breast Cancer

Shopnil Akash [1], Ajoy Kumer [2], Akhel Chandro [3], Unesco Chakma [4], Mohammed Mahbubul Matin [5,*]

1 Department of Pharmacy, Daffodil International University, Sukrabad, Dhaka, 1207, Bangladesh; shopnil.ph@gmail.com (S.A);
2 Laboratory of Computational Research for Drug Design and Material Science, Department of Chemistry, European University of Bangladesh, Dhaka, 1216, Bangladesh; ajoy@eub.edu.bd (A.K);
3 Department of Poultry Science, Faculty of Animal Science & Veterinary Medicine, Sher-e-Bangla Agricultural University, Dhaka, Bangladesh; akhel.sau6012@gmail.com (A.C);
4 Department of Electrical and Electronic Engineering, European University of Bangladesh, Gabtoli, Dhaka, 1216, Bangladesh; unescochakma@gmail.com (U.C.);
5 Bioorganic and Medicinal Chemistry Laboratory, Department of Chemistry, Faculty of Science, University of Chittagong, Chittagong, 4331, Bangladesh; mahbubchem@cu.ac.bd (M.M.M.);
* Correspondence: mahbubchem@cu.ac.bd (M.M.M.);

Scopus Author ID 7006284929
Received: 17.06.2022; Accepted: 30.070.2022; Published: 8.10.2022

Abstract: D-glucofuranose has potent bioactivity against numerous diseases and pathogens, such as bacteria, fungi, viruses, and cancer. Normally, the ketal form of D-glucofuranose is converted into the non-ketal form by drug metabolism in the human body; as a result, both the ketal and non-ketal forms of D-glucofuranose are considered. To make a comparative biological activity study of ketal and non-ketal species of nine derivatives of D-glucofuranose, two bacteria, black fungus, white fungus, and triple-negative breast cancer, were selected. Firstly, the PASS prediction data from the online PASS tool indicated the probability of pathogenic efficacy through the Pa and Pi parameters. Secondly, the computational studies, such as molecular docking, molecular dynamic, ADMET, drug-likeness, pharmacokinetic, aquatic, and non-aquatic features, were calculated with three FDA-approved drugs, including azithromycin, nystatin, and cyclophosphamide. A comparative study of computational data has been performed where the ketal forms of D-glucofuranose derivatives were found highly biologically active with the satisfaction of the pharmacokinetic parameters, ADMET parameters, and Lipinski rule.

Keywords: antimicrobials; docking; molecular dynamics; pharmacokinetic properties; triple-negative breast cancer.

1. Introduction

In the age of modern medical science, chemists, biologists, pharmacologists, and scientists are focused on carbohydrate-containing molecules and their analogs to develop and discover potential medications [1]. Carbohydrates are the largely unexplored reservoir of potential therapeutic development; consequently, they hold promise for the future of medicine

[2,3]. These sugar compounds have employed and recognized potential medications against various pathogens, such as antibacterial [4], antifungal [5], anticancer [6], antiviral [7], anti-diabetic [8], and anti-inflammatory [9]. Thus, many acylated monosaccharides and their derivatives have been studied as a wide spectrum of biological efficacy from 2004 through 2022 by Matin *et al*. [10-12], whereas Kabir *et al*. introduced the same concept in an earlier period in this field [13].

Computational research has addressed acylated monosaccharides' structure-activity relationship (SAR), which has wide applications in biomedical and pharmaceutical research. Computer-aided design of molecules or computational chemistry, reaction processes, reaction kinetics, and drug design has become the most sought-after research tool in the modern period due to their immense advantages [14]. First and foremost, it has been shown that Walton Kohn's 1990 development of density functional theory (DFT) [15] is among the most effective methods for accurately determining the electronic and nuclear structural magnitudes [16]. Furthermore, DFT has been used to forecast the structural relationship of HOMO and LUMO, which are indicators of chemical compounds' chemical stability and sensitivity, respectively [17]. Molecular modeling has become the most trusted reference for chemists, biologists, pharmacologists, and scientists designing new drug molecules. It adds to the fulfillment of biochemical properties by interacting and building numerous interactions between proteins and organic compounds [18]. The complementary field of molecular modeling methodologies means that the reactivity environment for organic, metallic, and bio-molecules via biochemical systems is characterized by reactive oxygen species (ROS) [19].

In recent years, researchers worldwide have focused a great deal of emphasis on this field for various investigations, including medication development and the conceptual exploration of bioactive compounds using DFT and other functional approaches [20]. Since its most significant benefits pertain to different activities, the first and most crucial utilization of computational models is to shorten the time required in the laboratories undertaking numerous experimental processes to create medications in the clinical [21]. For example, for developing a new drug molecule, there have conducted various tests in the laboratory, ensuring that a drug candidate is potentially and therapeutically safe. After that, they have been selected for further analysis, which requires at least three to five years to preselect a candidate for the drug. If any operation or characteristics of the therapeutic candidate is rejected in the laboratory throughout this evaluation, the whole time allotted for this research would be wasted. Furthermore, when conducting all these tests, researchers and discoverers utilize a large number of chemicals and materials which are expensive and harmful to the environment if disposed to aquatic and non-aquatic environments [22].

Consequently, the field of computational methods is fast expanding, providing more detailed findings of the system's behavior under different conditions, often for cases in which intuitive analytical solutions are unavailable. Besides, *in silico* studies are now more common in predicting the chemical descriptors, molecular docking, ADMET characteristics, drug-likeness, etc., to demonstrate the pharmacological background of pathogens. These tools are helpful in the gene expression analysis and elucidate biological mechanisms, including the drug development process. All these encouraging and significant results led us to apply molecular modeling or computational methods in the present investigation/study.

2. Computational Details

2.1. Optimization and ligand preparation.

Firstly, all the chemical structures were drawn with the help of Chemdraw Professional. The optimization of these compounds has been completed by utilizing vibrational frequencies from the B3LYP functional and DND basis (diffused basis set) semi-core pseudo-potentials [23], and the series of 18 derivative molecules of ketal and non-ketal have been saved to the pdb file for further computational studies such as molecular docking, molecular dynamics, and ADMET properties, etc.

2.2. PASS prediction.

PASS is a toolset that forecasts 565 potential bioactivities of a molecule based on its structure and chemical composition [24]. It has been performed and collected data with the help of the Pass online website http://way2drug.com/PassOnline/predict.php. This web server can predict antibiotics, antidepressants, antiviral (AIDS), contraceptives, tumor necrosis factors, antifungal, antibacterial, and many more are among these properties. All these characteristics are the fundamental requirement for new drug development [25].

2.3. In silico pharmacokinetics ADMET and drug-like parameters prediction.

The ADMET characteristics were designed to identify promising drug contenders by predicting pharmacokinetics, biophysical, and drug-like characteristics in the early clinical drug development and discovery stages [26]. This method allows researchers to determine pharmacokinetic parameters (ADMET), such as the amount of drug absorbed by the human intestine, the amount of drug that crosses the blood-brain barrier, and the amount of drug that enters and exits the central nervous system [27]. In addition, the metabolism of a medication reflects the biochemical bioconversion of medicine by the bloodstream, the total clearance of medications, and the toxic effects limits of the substances [28,29].

2.4. Protein preparation.

The 3D structure of two pathogenic bacteria (PDB IDs 5YHG and 1DIH), two fungi (PDB IDs 6DEQ and 5B8I), and two triple-negative breast cancer protein fungi (PDB IDs 5ha9 and 4pv5) were acquired from the protein data bank "https://www.rcsb.org/" in the pdb file format [30]. The PyMol (version 1.3) program removes all heteroatoms and water molecules [31]. Protein-energy minimization was achieved using the Swiss-Pdb viewer program version 4.1.0 [32]. Next, molecular docking studies were performed on the optimized compounds against these different protein targets.

2.5. Molecular docking study and visualization.

The PyRx program (version 0.8) was used to create the protein and the ligand's molecular docking interaction [33]. We utilized AutodockVina Tools (ADT) from the PyRx software suite to import proteins and associated ligands for docking investigation. The grid box size in AutoDockVina was set based on protein, and it has been listed below in Table 1 for a different protein. After docking was concluded, both the macromolecule and ligand frameworks were stored in the pdbqt format specified by Biovia Discovery Studio 2020 to

investigate and illustrate the docking outcome and lookup for the non-bonding interactions between ligands and amino acid residues of the receptor protein [34].

Table 1. Grid box parameters used for docking analysis in this study for bacteria.

Protein Name with the PDB ID	Grid box size	
	Dimension (Å)	Center
1DIH	X: 50.213	X: 21.84
	Y: 44.143	Y: 7.1839
	Z: 66.903	Z: 29.7499
5YHG	X: 63.912	X: 109.093
	Y: 87.855	Y: 17.117
	Z: 52.949	Z: 51.427
6DEQ	X: 82.573	X: 29.154
	Y: 54.122	Y: 95.319
	Z: 780909	Z: 131.42
5B8I	X: 68.409	X:31.994
	Y:91.868	Y:44.689
	Z: 77.064	Z:10.346
5HA9	X: 83.052	X: -4.0485
	Y: 72.240	Y: 11.0079
	Z: 89.276	Z: -21.4322
4PV5	X: 46.011	X = -3.4569
	Y:55.660	Y: 5.9539
	Z:62.007	Z: 13.9701

2.6. Molecular dynamics.

Nanoscale Molecular Dynamics (NAMD) application has been used to execute molecular dynamics on a desktop or laptop computer, either dynamically with the live stream or in batch mode [35]. The molecular dynamics (MD) simulation has been used to support the docking data achieved for the optimum and Potential medications and the targeted protein up to 100 ns for holo-form (drug-protein) using the AMBER14 force field, which was applied to the docking findings [36]. During the simulation, a cubic cell was replicated within 20 Å on each side of the corresponding boundary circumstance. Finally, root-mean-square deviation (RMSD) and root-mean-square fluctuation (RMSF) were determined with the aid of Visual Molecular Dynamics (VMD). After equilibration with 0.9 percent NaCl at 298 K temperature and concentration of a solvent, the scheme was re-equilibrated with liquid.

2.7. Calculation of QSAR and pIC_{50}.

A number of distinct electronic descriptors are generated when utilizing the electronic density approach to describe the studied substances' structure-activity correlation and chemical reactivity. Among them, the quantitative structure-activity relationship (QSAR) is a statistical simulation tool for identifying correlations between structural features of bioactive molecules and bioactivity features [37]. The QSAR and pIC_{50} data have been assessed with the aid of Chemdesk and a trusted algorithm called multiple linear regression (MLR). This free database provides us with the required data (including Chiv5, MRVSA9, and PEOEVSA5) for calculating QSAR and pIC50 [38].

3. Results and Discussion

3.1. Optimized structures of the tested ligands.

Molecular atoms are always moved to achieve the most stable configuration with the lowest feasible ground energy state. So, geometry optimization has been achieved using density functional theory (DFT). DFT is mainly a computational quantum mechanical modeling tool that may be used in physics, chemistry, and materials science to evaluate the stability of a molecular structure [39]. The optimized chemical structures of these derivatives are represented in Figure 1.

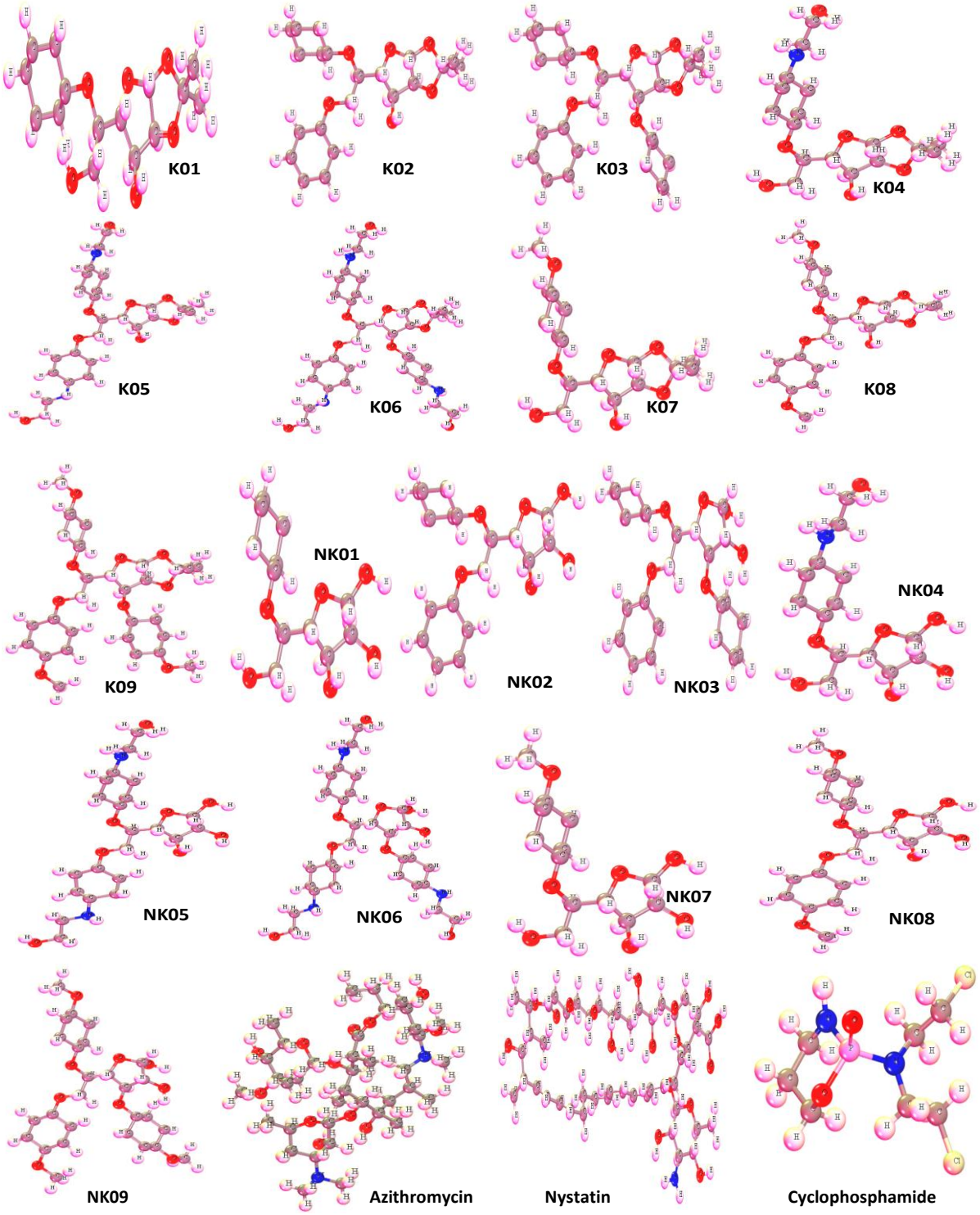

Figure 1. DFT optimized structures of ketal and non-ketal glucofuranoses.

3.2. Lipinski rule, pharmacokinetics, and drug-likeness.

Drug-likeness is determined by Lipinski's rule of five, which states that any chemical molecule having a wide range of pharmacological functions must have chemical and physical characteristics that make it probable to be biologically effective or orally active in humans. In 1997, Christopher A. Lipinski came up with the rule reflected in the fact that almost all orally delivered medications are smaller and slightly lipophilic [30,41]. So, it is vital to consider during drug development when a potent bioactive lead molecule is modified step-by-step to enhance the affinity and specificity of the molecule and to ensure drug-like biophysical characteristics are retained, as represented by Lipinski's rule [42]. An orally administered medicine must meet the following features for Lipinski's rule to implement: the hydrogen bond donor should be less than five, and the hydrogen bond acceptor should be less than ten with a molecular mass of less than 500 Dalton [40].

In the above criteria, almost all the newly developed ketal and non-ketal compounds have fulfilled the Lipinski rule, excluding ligands, K06 and NK06 didn't follow the Lipinski rule due to higher molecular weight (MW>500) (Table 2). The range of MW reported has been found to be 256.25-625.71, where the largest MW is 625.71 & 585.65, and these two do not follow the rule of five of Lipinski. Secondly, K06 and NK04, NK05, and NK06 are the only chemicals poorly absorbed in the gastrointestinal system with lower oral bioavailability. In most cases, the bioavailability range has been seen as 0.55. So, these drugs should be recommended for further use.

Table 2. Data of Lipinski rule, pharmacokinetics, and drug-likeness.

Ligand No.	NBR	HBA	HBD	TPSA[1], Å²	Consensus Log Po/w	Log Kp (skin permeation), cm/s	Lipinski rule		MW	Bioavailability Score	G.I. absorption
							Result	Violation			
Ketal form											
K01	04	06	02	77.38	0.95	-7.56	Yes	00	296.32	0.55	High
K02	06	06	01	66.38	2.59	-6.36	Yes	00	372.41	0.55	High
K03	06	08	00	55.38	4.25	-5.15	Yes	00	448.51	0.55	High
K04	07	07	04	109.44	0.42	-8.42	Yes	00	355.38	0.55	High
K05	12	08	05	130.90	1.46	-8.07	Yes	00	490.55	0.55	High
K06	17	09	06	152.16	2.55	-7.72	No	03	625.71	0.17	Low
K07	05	07	02	86.61	1.05	-7.77	Yes	00	326.24	0.55	High
K08	08	08	01	84.84	2.72	-8.76	Yes	00	432.46	0.55	High
K09	11	09	00	83.07	4.38	-5.76	Yes	01	538.59	0.55	High
Non-Ketal form											
NK01	04	06	04	99.38	-0.40	-8.42	Yes	00	256.25	0.55	High
NK02	06	06	03	88.38	1.20	-7.22	Yes	00	332.25	0.55	High
NK03	08	06	0	77.38	3.00	-6.02	Yes	00	408.44	0.55	High
NK04	07	07	06	131.64	0.98	-9.28	Yes	01	315.32	0.55	Low
NK05	12	08	07	152.90	0.20	-8.93	Yes	01	450.48	0.55	Low
NK06	17	09	08	174.16	1.19	-8.59	No	03	585.65	0.17	Low
NK07	05	07	04	108.61	-0.51	-8.63	Yes	00	286.28	0.55	High
NK08	08	08	03	106.84	1.33	-7.63	Yes	00	392.40	0.55	High
NK09	11	09	02	105.2	03	-6.62	Yes	00	498.52	0.55	High
Azithro-mycin	07	14	05	180.08	2.02	-8.01	No	02	748.98	0.17	Low
Nystatin	03	18	12	319.61	-0.18	-12.09	No	03	926.1	0.17	Low
Cyclopho-sphamide	05	04	01	51.380	1.23	-7.45	Yes	00	261.09	0.55	High

[1] TPSA: Topological polar surface area; Consensus Log: Logarithm of partition coefficient between n-octanol and water; NBR: Number of rotatable bonds; HBA: Hydrogen bond acceptor; HBD: Hydrogen bond donor; MW: Molecular weight; G.I. Absorption: Gastrointestinal absorption.

3.3. PASS prediction.

Using the web, we have estimated the antiviral, antibacterial, antifungal, antibiotic, and antineoplastic characteristics of all synthesized ketal and non-ketal derivatives K01–K09 & NK01-NK09 application PASS (http://www.pharmaexpert.ru/passonline/) [43,44]. The following Table 3 shows the PASS outcomes for Pa and Pi, which have been seen from data for synthetic derivatives of ketal and non-ketal. The largest Pa value has been found to be 0.405 for antiviral in ligand **NK01**, the antibacterial largest Pa is 0.435 in ligand in **NK01** and **NK07**, and in antifungal, the largest Pa is 0.568 in **K01** (Table 3).

The last two are antibiotic and antineoplastic; in this case, the largest Pa score is 0.263 in **K01**, and the largest Pa score is 0.704 in ligand **K07** for antineoplastic. Our findings showed that these compounds were more effective towards antineoplastic, antibacterial, and fungi pathogens than viral pathogens and antibiotics. So, in this research, two pathogenic bacteria, fungi, and two triple-negative breast cancer proteins have been taken for further computational studies, such as molecular docking, MD, etc.

Table 3. Data of PASS prediction of ketal and non-ketal compounds.

Ligand No.	Antiviral		Antibacterial		Antifungal		antibiotic		Antineoplastic	
	Pa	Pi	Pa	Pi	Pa	Pi	Pa	Pi	Pa	Pi
Ketal (**K01**)	0.225	0.076	0.431	0.024	0.568	0.022	0.263	0.018	0.684	0.029
K02	0.202	0.093	0.425	0.025	0.550	0.024	0.219	0.024	0.605	0.044
K03	0.316	0.220	0.337	0.047	0.382	0.054	0.153	0.047	0.278	0.166
K04	0.176	0.126	0.372	0.036	0.399	0.050	0.194	0.030	0.677	0.030
K05	0.169	0.136	0.373	0.037	0.390	0.052	0.160	0.043	0.607	0.044
K06	0.275	0.110	0.283	0.067	0.237	0.114	0.098	0.084	0.355	0.123
K07	0.194	0.101	0.431	0.024	0.561	0.022	0.266	0.018	0.704	0.025
K08	0.177	0.024	0.425	0.025	0.543	0.024	0.223	0.024	0.638	0.037
K09	0.318	0.079	0.337	0.047	0.373	0.056	0.156	0.045	0.340	0.130
Non-Ketal (**NK01**)	0.405	0.033	0.435	0.024	0.423	0.045	0.269	0.017	0.381	0.112
NK02	0.387	0.041	0.429	0.024	0.396	0.050	0.227	0.023	0.252	0.184
NK03	0.299	0.092	0.399	0.030	0.367	0.058	0.195	0.030	0.240	0.190
NK04	0.331	0.071	0.376	0.036	0.238	0.113	0.200	0.028	0.454	0.086
NK05	0.322	0.077	0.378	0.036	0.231	0.117	0.165	0.040	0.350	0.125
NK06	0.211	0.165	0.338	0.046	0.205	0.131	0.132	0.058	0.335	0.133
NK07	0.394	0.038	0.435	0.024	0.414	0.047	0.272	0.017	0.450	0.087
NK08	0.373	0.048	0.429	0.024	0.387	0.053	0.230	0.023	0.325	0.138
NK09	0.279	0.106	0.400	0.030	0.358	0.060	0.198	0.029	0.308	0.148
Azithromycin	0.723	0.001	0.964	0.000	0.723	0.009	0.941	0.000	0.416	0.098
Nystatin	0.210	0.087	0.967	0.000	0.986	0.000	0.946	0.000	0.762	0.17
Cyclophosphamide	0.200	0.177	N/A	N/A	N/A	N/A	N/A	N/A	0.996	0.003

3.4. Molecular orbitals and chemical reactivity descriptors.

Molecular orbitals and chemical reactivity descriptors are mathematical approximations of the characteristics of chemical structures developed by the computational system. Table 4 shows the listed compounds' calculated LUMO, HOMO, and E gap, chemical potential, electronegativity, hardness, softness, and electrophilicity. These estimates data have been computed using the B3LYP functional. In displayed Table 4 reveals that the HOMO–LUMO gap ranges from 6.516 to 8.352 eV for all investigated derivatives, with NK03 having

a lower energy deficit and the maximum softness level & minimum hardness level. The HOMO-LUMO energy difference determines the molecule's chemical reactivity, and the significant HOMO-LUMO gap indicates greater kinetic with poor chemical durability [45-48].

Table 4. Data of chemical descriptors.

S/N	A = -LUMO	I = - HOMO	Energy = I-A	Electronegativity $(\chi) = \frac{I+A}{2}$	Chemical potential $(\mu) = -\frac{I+A}{2}$	Hardness $(\eta) = \frac{I-A}{2}$	Softness $(\sigma) = \frac{1}{\eta}$	Electrophilicity $(\omega) = \frac{\mu^2}{2\eta}$
K01	-1.242	-9.437	8.095	-5.2895	5.2895	-4.0475	-0.2471	-3.4563
K02	-1.107	-9.127	8.020	-5.117	5.117	-4.01	-0.2494	-3.2648
K03	-1.267	-9.071	7.804	-5.169	5.169	-3.902	-0.2563	-3.4237
K04	-1.031	-8.831	7.80	-4.931	4.931	-3.90	-0.2564	-3.1173
K05	-1.307	-8.767	7.460	-5.037	5.037	-3.73	-0.2681	-3.4010
K06	-1.316	-8.682	7.366	-4.999	4.999	-3.683	-0.2715	-3.3926
K07	-1.159	-9.237	8.078	-5.198	5.198	-4.039	-0.2476	-3.4048
K08	-1.171	-9.102	7.931	-5.1365	5.1365	-3.9655	- 0.2522	-3.3266
K09	-1.49	-9.089	7.599	-5.2895	5.2895	-3.7995	-0.2632	-3.6819
NK01	-0.985	-9.337	8.352	-5.161	5.161	-4.176	-0,2375	-3.1892
NK02	-1.144	-9.149	8.193	-5.2405	5.2405	-4.0965	-0.2441	-3.3520
NK03	-1.71	-8.226	6.516	-4.968	4.968	-3.258	-0.3069	-3.7878
NK04	-1.019	-8.815	7.796	-4.917	4.917	-3.898	-0.2565	-3.1012
NK05	-1.586	-8.688	7.102	-5.137	5.137	-3.551	-0.2816	-3.7157
NK06	-1.588	-8.561	6.971	-5.0745	5.0745	-3.4865	-0.2868	-3.6929
NK07	-1.144	-9.217	8.073	-5.1805	5.1805	-4.0365	-0.2477	-3.3242
NK08	-1.209	-9.094	7.885	-5.1515	5.1515	-3.9425	-0.2536	-3.2556
NK09	-1.787	-8.975	7.188	-5.381	5.381	-3.594	-0.2782	-4.0283
Azithromycin	-0.40	-9.14	8.740	-4.77	4.77	-4.37	-0.2288	-2.6033
Nystatin	-0.822	-7.16	6.294	-3.969	3.969	-3.147	-0.3178	-2.5029
Cyclophosph-amide	-1.351	-9.945	8.594	-5.648	5.648	-4.297	-0.2327	-3.7119

3.5. Frontier molecular orbitals (HOMO and LUMO).

The frontier molecular orbital (FMO) has been used to assess the chemical reactivity of compounds and the engaged regions of drug peptides where they have been bounded with each other. The FMO has arranged the diagram in Figure 2. The negative terminal of orbitals is yellow in LUMO, whereas the positive terminal is green in HOMO. On the other hand, the deep maroon hue for HOMO denotes a positive orbital terminal, whereas the bright greenish shade represents a negative orbital terminal in LUMO. The smaller energy gap assists in forming an engagement between medicines and the targeted protein.

There are no special frontier molecular orbital (FMO) trends in D-glucofuranose derivatives' ketal and non-ketal forms. In the case of the ketal form, none of HOMO and LUMO were found in the functional group, and these were found in the side chains, which is similar to the non-ketal form of D-glucofuranose derivatives.

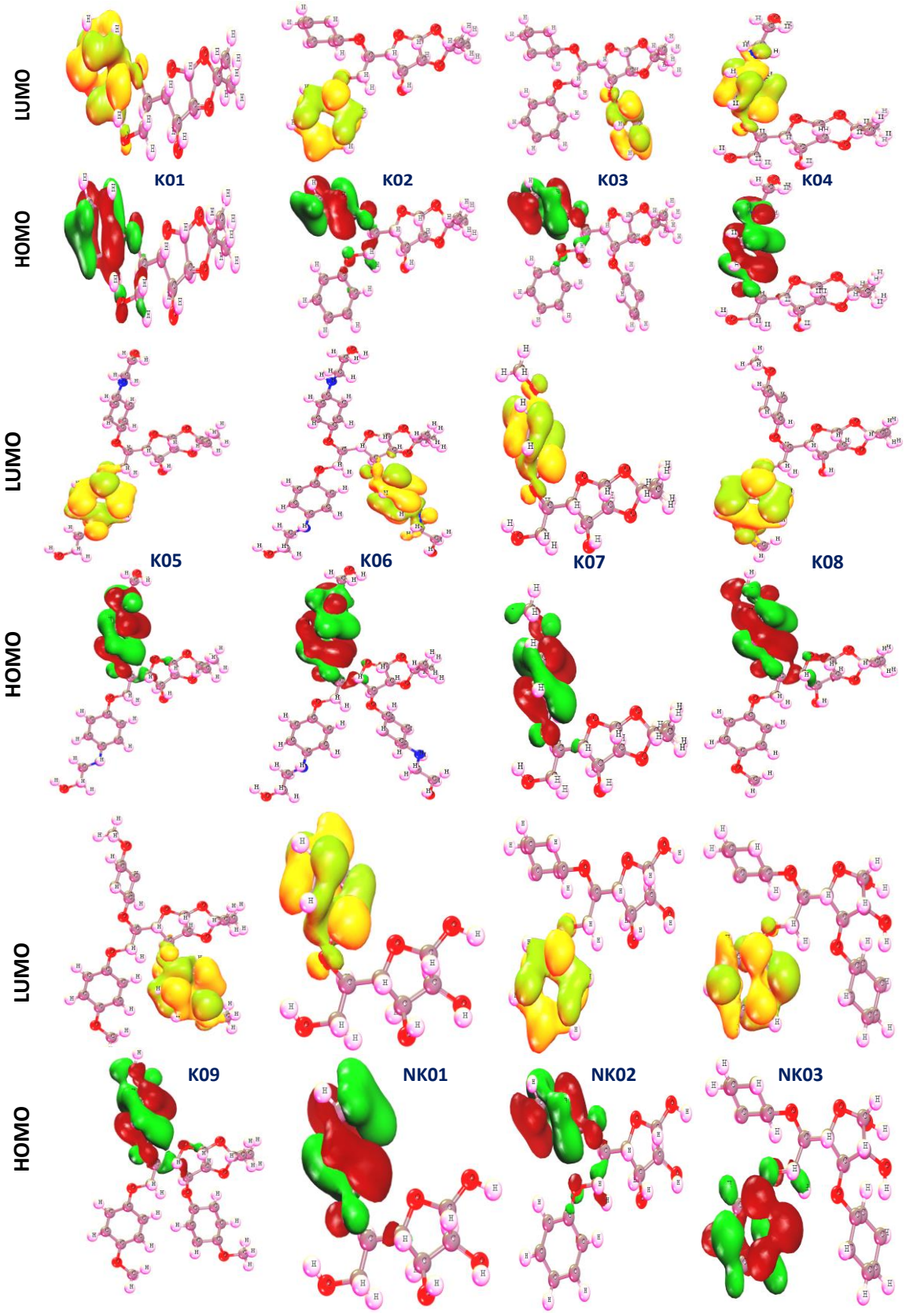
LUMO
HOMO
K01
K02
K03
K04
LUMO
HOMO
K05
K06
K07
K08
LUMO
HOMO
K09
NK01
NK02
NK03

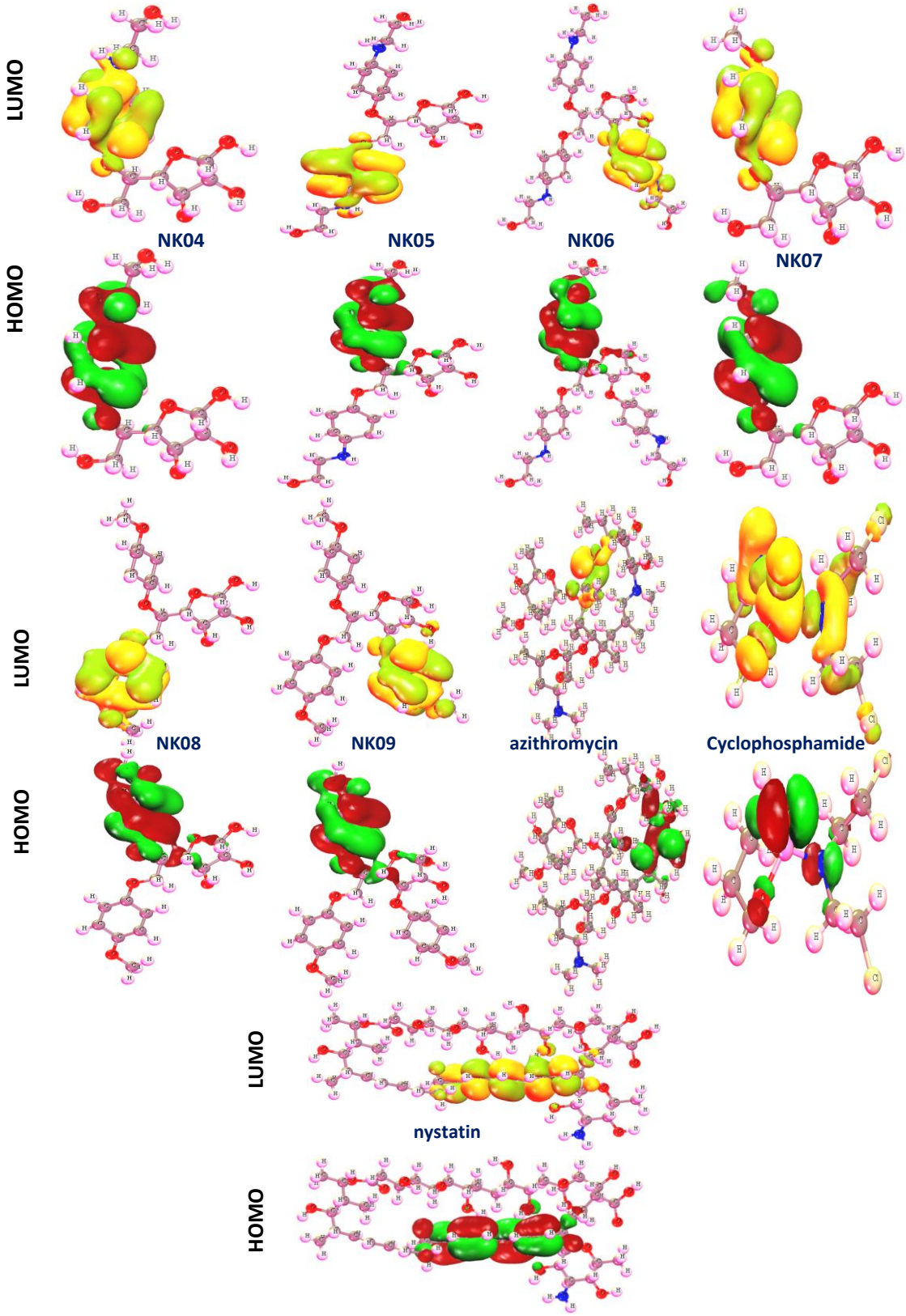

Figure 2. HOMO and LUMO diagram of the compounds.

3.6. Molecular of Electrostatic Potential (MEP) charge distribution mapping.

The electrostatic potential has been correlated to dipole moment, electronegativity, and partial charges. It creates the comparative polarization of chemical structure. It is an important and valuable method of accessing chemical structure's totally positive and negative charges and how they are organized across the molecules. The positive portion has designed the blue color, and the red portion has been designed by the negative portion. The positive portion is

more significant than the negative charge since the blue color is higher in displaying all the chemical structures (Figure 3). It is understood that they have the strongest affinity to the nucleophilic groups in these compounds [49,50].

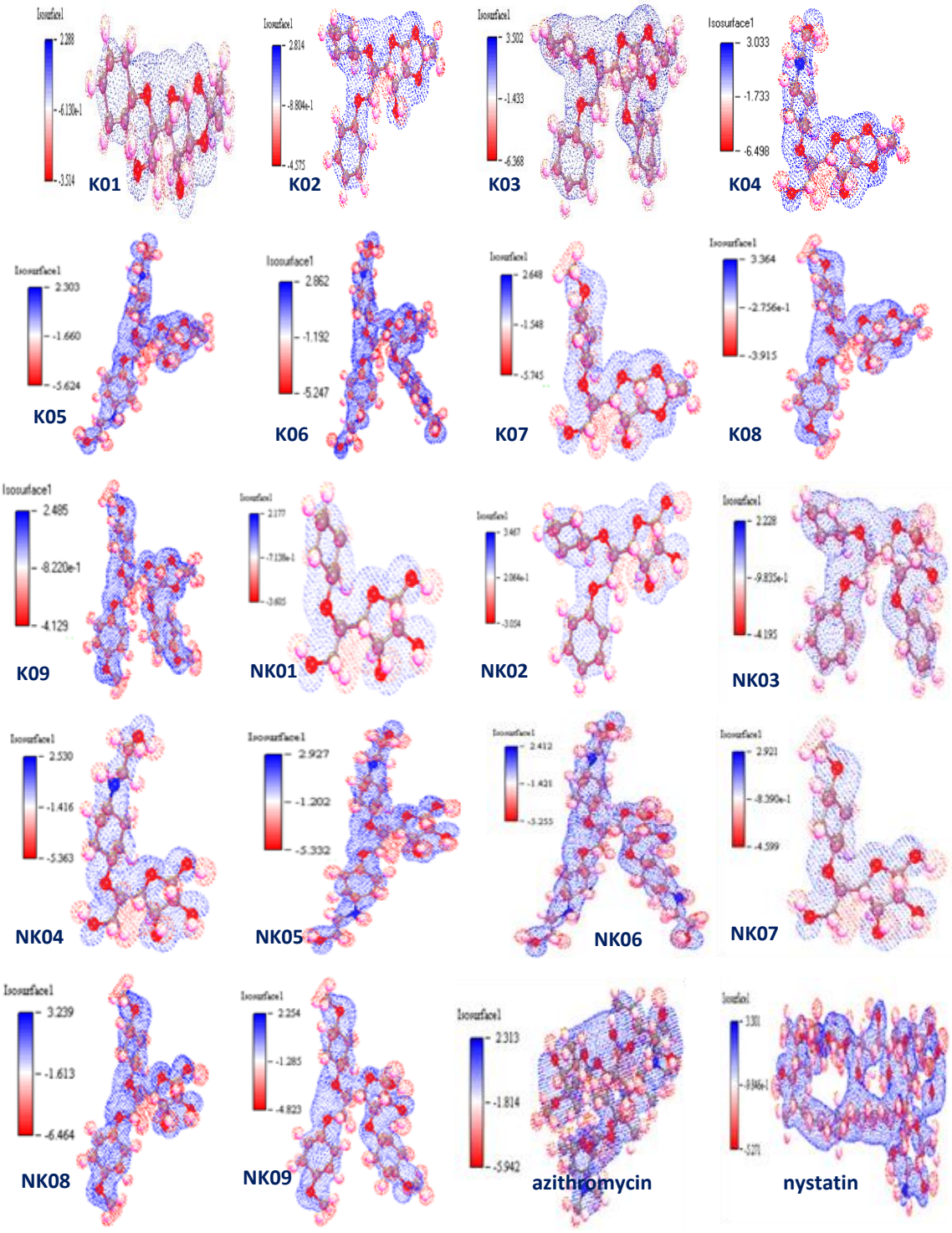

Figure 3. Molecular electrostatic potential (MEP) mappings.

3.7. Molecular docking against pathogenic bacteria

The computational concept of docking studies is widely used in structural biology and computer-aided drug development. The ultimate focus of molecular docking is to identify the probable binding orientations of a possible agonist or new drug molecule that has a recognized three-dimensional structure with a biological target employing computer simulations.

Specifically, in this study, a total of eighteen bioactive molecules were picked and separated into two categories (ketal and non-ketal), after which they were docked with six proteins (bacteria, fungi, and triple-negative breast cancer) to determine the most effective antagonist. As shown in Table 5, their binding energy experiment findings were favorable. In this work, three FDA-approved molecules were considered a starting point to compare with newly synthesized compounds (Azithromycin, PubChem CID 447043; Nystatin, PubChem CID 14960; Capecitabine, PubChem CID 60953). The study's main goal was to find the most effective synthetic molecule interacting stronger than standard FDA-approved agonists [51].

Table 5. Docking score against ketal and non-ketal groups with bacteria.

Ligands	*E. coli* (1DIH)			*Staphylococcus aureus* (5YHG)		
	Binding Affinity (kcal/mol)	**No of H bond**	**No of Hydrophobic bond**	**Binding Affinity (kcal/mol)**	**No of H bond**	**No of Hydrophobic bond**
Ketal (**K01**)	-7.0	03	03	-8.3	05	06
K02	-7.6	04	07	-9.1	05	05
K03	-8.4	02	05	-7.7	03	08
K04	-7.0	04	04	-7.3	04	06
K05	-7.6	08	07	-7.6	03	09
K06	-7.2	06	09	-8.5	06	12
K07	-7.1	02	05	-7.5	02	07
K08	-8.0	07	08	-8.2	03	09
K09	-8.3	04	12	-8.6	04	14
Non-Ketal (**NK01**)	-6.5	03	03	-8.3	02	01
NK02	-6.3	04	03	-8.3	06	05
NK03	-8.0	04	03	-8.0	01	03
NK04	-6.6	04	00	-7.4	03	03
NK05	-7.3	11	04	-7.5	01	05
NK06	-6.9	09	01	-7.6	06	06
NK07	-6.4	07	02	-8.1	04	06
NK08	-7.4	05	05	-7.1	04	01
NK09	-7.3	03	06	-7.8	03	14
Azithromycin	-8.2	02	03	-8.0	05	04

Here, the docking index of K03 against *E. coli* is -8.4 kcal/mol and -9.1 kcal/mol in K02 against *Staphylococcus aureus*. At the same time, FDA approved azithromycin showed -8.2 kcal/mol and -8.0 kcal/mol, correspondingly. The newly synthesized compounds had a larger affinity for the target bacterial pathogen than azithromycin.

3.8. Molecular docking against pathogenic fungi

The molecular docking score against pathogenic fungi also demonstrates better binding affinities than the standard drugs (Table 6). In this case, the range of binding affinities was -7.3 to -11.0 kcal/mol in the ketal group, and the highest binding energy was 11.00 kcal/mol against *Coccidioides immitis* in ligand K03, while the range in the non-ketal group showed -6.7 to -9.3 kcal/mol and the enormous affinity has been obtained -9.3 kcal/mol in ligand NK03 against *Coccidioides immitis*. At the same time, the standard nystatin represented -9.3 kcal/mol. So, there is no doubt the newly synthesized molecules are much better than the standard drugs [49].

Table 6. Docking score against ketal and non-ketal groups with fungi.

Ligands	*Coccidioides immitis* (5B8I)			*Candida albicans* (6DEQ)		
	Binding Affinity (kcal/mol)	**No of H bond**	**No of Hydrophobic bond**	**Binding Affinity (kcal/mol)**	**No of H bond**	**No of Hydrophobic bond**
Ketal (K01)	-8.0	02	09	-8.4	05	01
K02	-9.6	00	11	-7.3	01	01

Ligands	*Coccidioides immitis* (5B8I)			*Candida albicans* (6DEQ)		
	Binding Affinity (kcal/mol)	No of H bond	No of Hydrophobic bond	Binding Affinity (kcal/mol)	No of H bond	No of Hydrophobic bond
K03	-11.0	02	10	-7.2	02	03
K04	-7.8	05	05	-6.5	06	06
K05	-9.1	05	11	-6.4	09	00
K06	-9.5	01	09	-7.3	06	06
K07	-7.3	00	07	-6.5	05	07
K08	-8.5	07	09	-7.1	03	07
K09	-10.3	02	21	-7.3	05	05
Non-ketal (NK01)	-7.1	05	02	-6.7	01	03
NK02	-8.7	03	08	-7.4	07	03
NK03	-9.3	01	06	-7.4	02	05
NK04	-6.8	07	02	-6.8	05	01
NK05	-8.0	05	04	-8.0	05	01
NK06	-8.5	05	04	-7.9	08	05
NK07	-6.7	07	02	-6.7	09	02
NK08	-8.2	08	06	-6.8	04	02
NK09	-8.3	05	11	-7.4	05	02
Nystatin	-9.3	11	00	-8.8	09	00

3.9. Molecular docking against triple-negative breast cancer proteins

The antineoplastic range has been found to bring better results in PASS prediction value. So, two triple-negative breast cancer proteins have been taken and completed molecular docking. After that, it has been seen that the newly synthesized compounds have the strongest affinities in contrast with triple-negative breast cancer. In this case, we have taken Capecitabine, which is the first oral chemotherapeutic for anticancer drugs and has been approved by the Food and Drug Administration (FDA) [52,53] as a standard to compare with newly developed ligands and the ligand which we have designed are opposed to the Capecitabine. The binding energy of standard Capecitabine has been found at -7.9 kcal/mol against 5ha9, and -6.6 kcal/mol against 4pv5. But, the newly synthesized molecules K03 have shown -10.8 kcal/mol and NK09 -10.6 kcal/mol, which are much larger than the standard antagonist Capecitabine (Table 7).

Table 7. Docking score against ketal and non-ketal groups with triple-negative breast cancer.

Ligands	PDB ID: 5HA9			PDB ID: 4PV5		
	Binding Affinity (kcal/mol)	No of H bond	No of Hydrophobic bond	Binding Affinity (kcal/mol)	No of H bond	No of Hydrophobic bond
Ketal (K01)	-8.8	05	04	-7.2	01	09
K02	-10.2	00	04	-8.4	00	12
K03	-10.8	00	09	-8.2	00	05
K04	-8.8	09	03	-7.1	05	11
K05	-7.8	03	05	-7.4	01	14
K06	-7.3	03	03	-7.3	06	08
K07	-7.9	04	07	-7.2	02	11
K08	-9.9	01	09	-8.0	04	11
K09	-10.4	09	09	-8.3	01	08
Non-Ketal (NK01)	-7.5	06	02	-6.3	01	01
NK02	-9.1	03	04	-7.8	04	06
NK03	-9.7	04	03	-7.9	00	06
NK04	-7.9	04	02	-7.2	05	11
NK05	-9.1	06	02	-7.1	08	04
NK06	-9.4	10	03	-6.4	04	05
NK07	-7.5	07	02	-6.4	04	03
NK08	-9.6	05	07	-6.9	07	7
NK09	-10.6	11	03	-7.0	03	06
Capecitabine	-7.9	05	03	-6.6	03	03

3.10. Protein-ligand interactions

The purpose is to create and perfect non-covalent connections between ligands and peptides essential for new therapeutic drug discovery. Figure 4 shows how the ligands have connected with peptides and where an attachment has been created between medicines with protein of bacteria, fungus, and triple-negative breast with their pocket region. The Biovia discovery studio and Pymol version 2020 have been utilized to design and graphically represent the ligand peptide pocket.

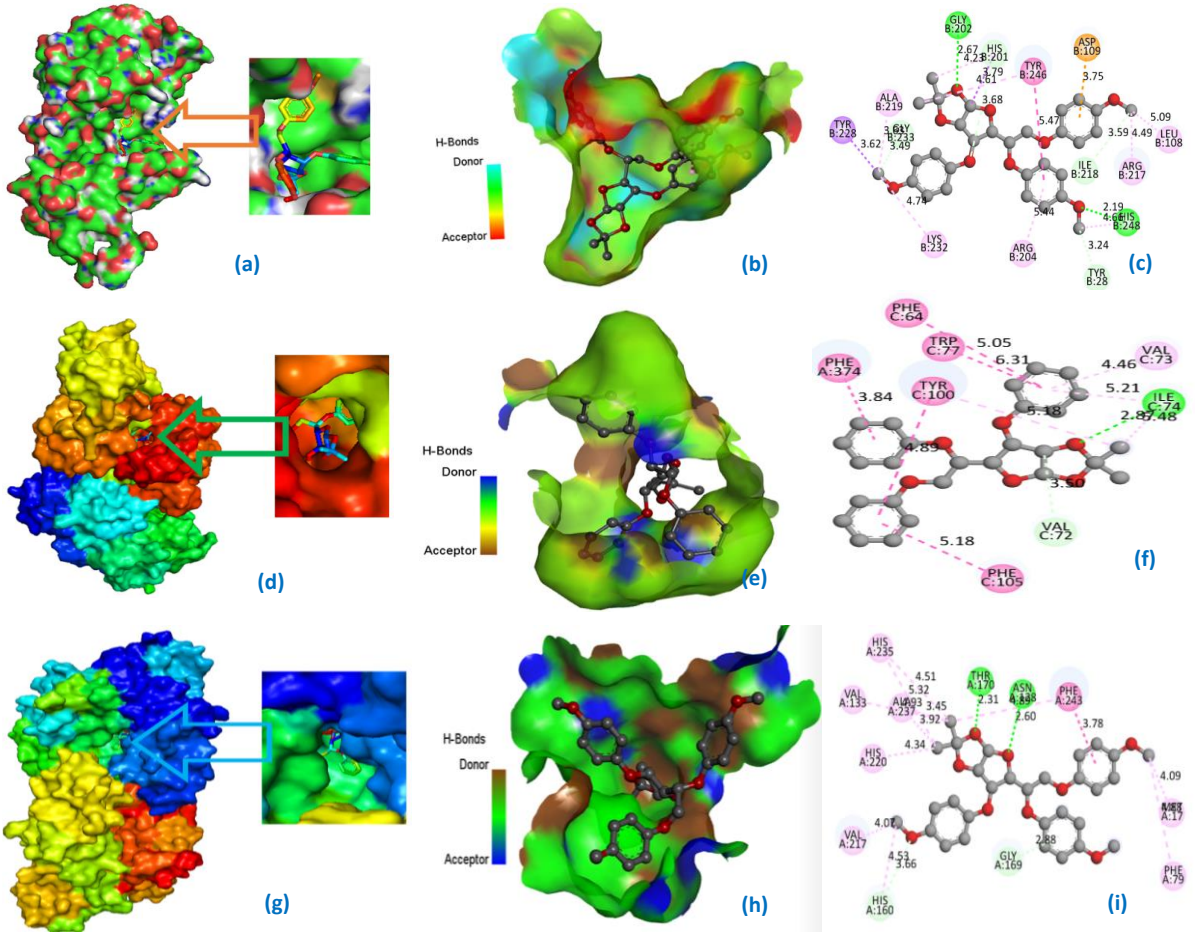

Figure 4. Protein-ligand interaction pocket: (a,b,c) *Staphylococcus aureus* (IDIH) with **K09**; (d,e,f) *Coccidioides immitis* (5B8I) with **K03**; (g,h,i) triple-negative breast cancer (5HA9) with **NK03**.

3.11. Molecular dynamics.

The molecular dynamics simulations include a platform for evaluation of the validity of the AutoDock protocol in terms of the average root-mean-square deviation (RMSD) and root-mean-square fluctuation (RMSF). Both RMSD and RMSF connect the protein's binding posture to the ligand. These are also employed to determine the mobility and stability of the ligand-protein complex [54,55]. RMSD of docked complexes should be smaller than 2 Å, indicating that the system is capable of effectively docking the compounds (excellent matching posture of ligand in drug site) [56]. Eventually, the RMSD established both the docked pose and that of docked complex straight to each other. A lesser RMSD value implies more precision and longevity of the docked mechanism [46]. These eighteen ketals and non-ketals docked compounds' longevity was characterized by ligand–protein RMSD, ligand-protein coupling, hydrogen bonding, and ligand-RMSF. In this work, the RMSD was estimated using the time (0-100 ns) and the interactions between amino acid residues of the protein.

In the protein of bacteria (pdb id 5YHG), the RMSD value is 0.7 Å in time 20 ns for all ligands, including standard azithromycin. But, while the time is increased up to 100 ns, the RMSD remains constant for NK02 (Figure 5). But, the other compounds have reached 0.9 Å. Similarly, the RMSD & RMSF has found 0.8 Å amino acid vs. residues.

The second one is a fungal protein (pdb id 5b8i); the RMSD has been found to be 0.8 Å at the early stages of time 20 ns. But, the RMSD has been seen to be different for each compound when the time is increased up to 100 ns, such as K03, NK02 & K09 show 0.8 Å while the ligands NK09 & Azithromycin have reported 0.9 Å. At the same time, the RMSD vs. amino acid residue has been seen at 0.8 Å in NK02, and the other compounds show 0.9 Å. But, the RMSF value has been seen as 0.7 Å for all complexes.

The last one is MD simulation for triple-negative breast cancer. In this simulation, it has been seen the RMSD has reached the maximum, which is 1.0 Å, both RMSD vs. Time and RMSD vs. amino acid residue (Figure 5). But, the RMSF is lower compared to RMSD, which is 0.6 Å for NK02 and 0.7 Å for other ligands.

It concluded that all the ligands' RMSD and RMSF value ranges had been found to be 0.6 Å -1.0 Å, much lower than the standard fitting pose. So, it can be said that all the ligand binds with peptides or pockets of protein accurately, and their stability is also excellent, which signifies the standard drug.

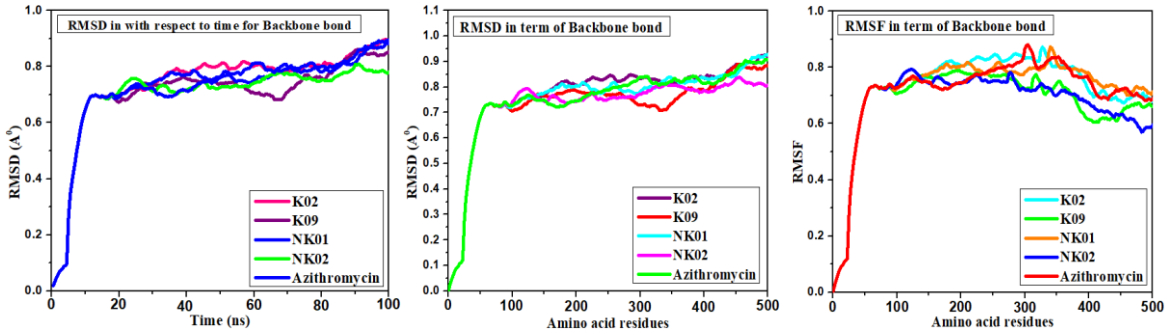

MD simulation of bacteria (5yhg) with ketal and non-ketal compounds

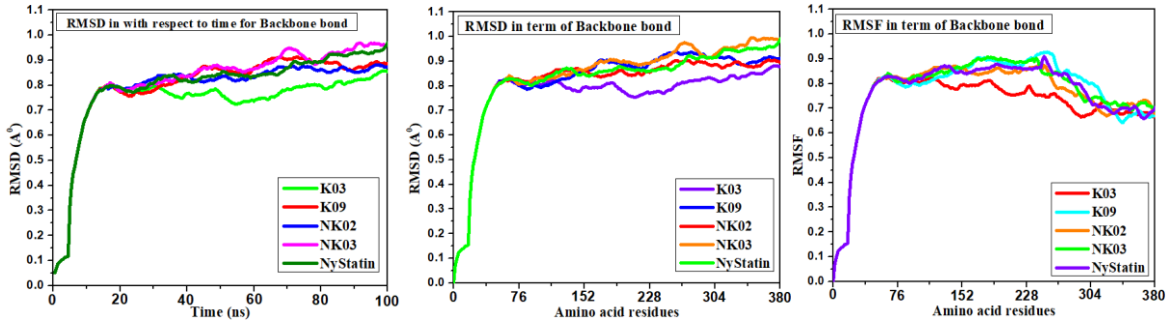

MD simulation of fungus (PDB id: 5b8i) with ketal and non-ketal compounds

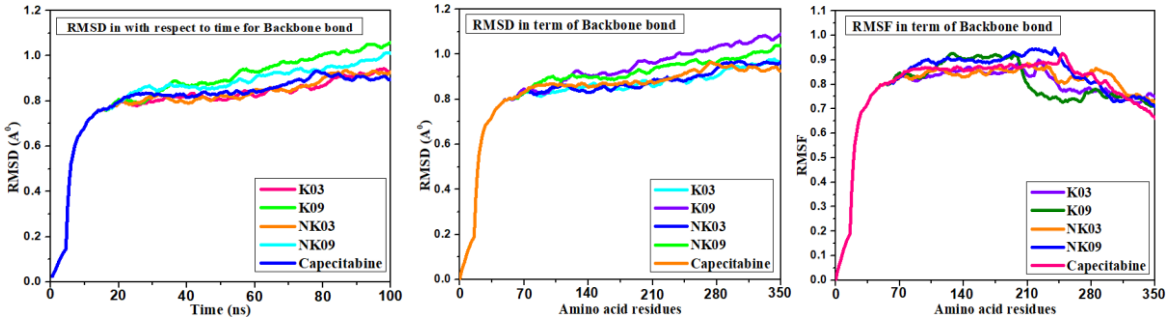

MD simulation of triple-negative breast cancer (5ha9) with ketal and non-ketals

Figure 5. Molecular dynamics (MD) simulation.

3.12. Comparative study of docking score between ketal and non-ketal form of molecules

In this study, computational studies have been conducted for the compounds K01-K09 and NK01-NK09 to compare their performance before and after reaching a physiological system. This is because ketal compounds contain an acid-sensitive acetonide group, which could be open in physiological systems [57].

So, to provide a basic comparison, the K01-K09 and NK01-NK09 ligands have been docked among two bacteria, two black and white fungal strains, and triple-negative breast cancer to determine their binding interactions (Figure 6). The bar diagram displayed the comparison between the outcomes of the ketals and non-ketals. It could be concluded that the binding affinity of ketal molecules is better than the non-ketal form against bacteria, black fungus, and triple-negative breast cancer. Still, the binding affinity against white fungus is almost identical to the ketal and non-ketal groups.

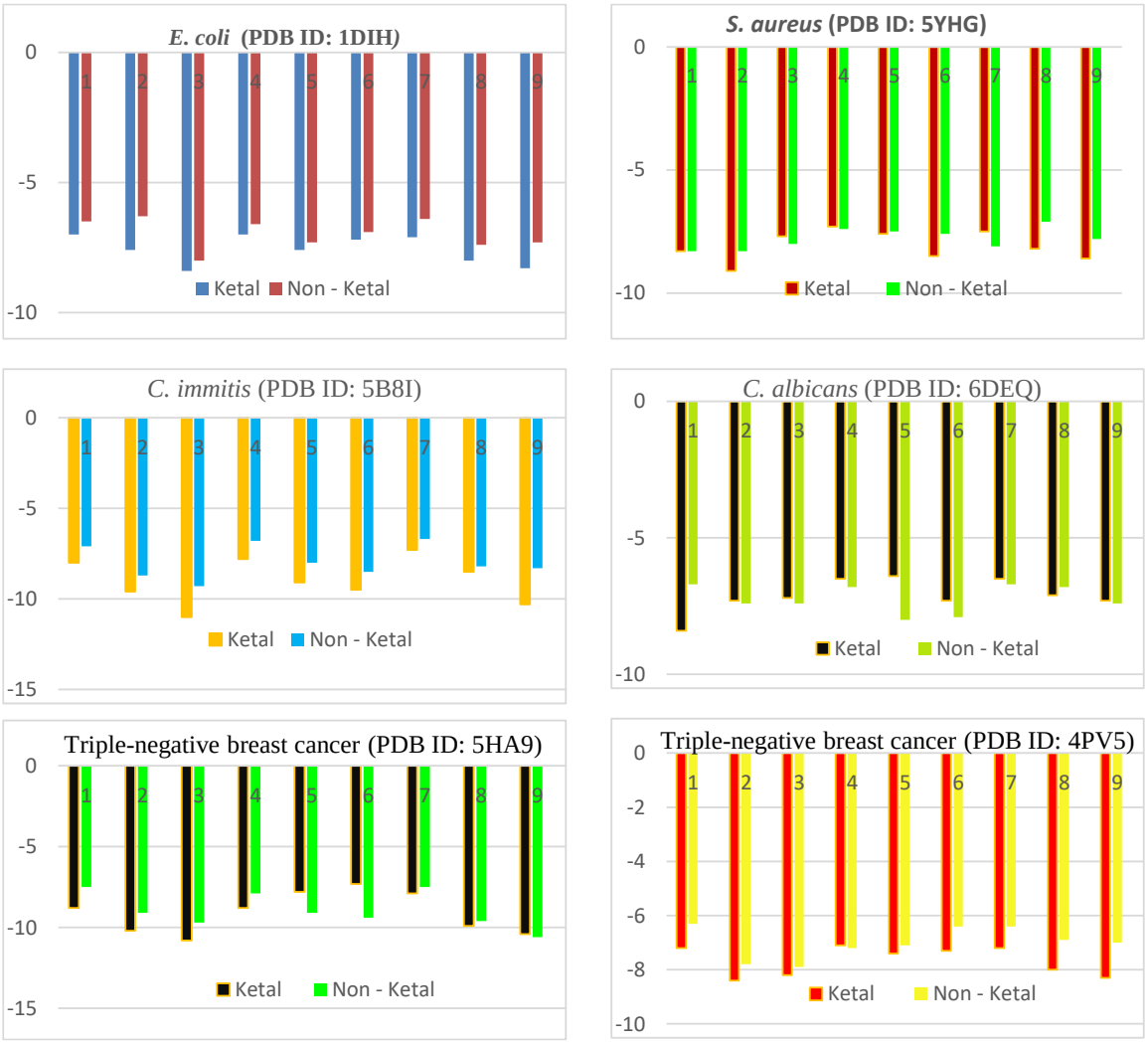

Figure 6. Docking score comparison between ketals and non-ketals.

In the case of molecular docking, the ketal form shows an almost high value of docking score. However, in molecular dynamics, the average value of root-mean-square deviation (RMSD) and root-mean-square fluctuation (RMSF) values of the docked complexes are used to assess the mobility and stability of the compounds. There are no accountable differences between RMSD and RMSF values for both ketal and non-ketal forms. The docked complexes of both the ketal and non-ketal forms convey similar stability.

3.13. ADMET studies.

ADMET is an acronym for Absorption, Distribution, Metabolism, Excretion, and Toxicity. Approximately 40-60 percent of all medications in clinical trials rapidly deteriorate to ADMET property predictive performance; hence this is a critical and essential step in the new drug design and discovery [58,59]. Although previously ADMET methods have been deployed at the end of a drug development stage, ADMET is currently deployed early stages of the drug development cycle to exclude compounds with inadequate ADMET features from the development stages, which results in a substantial reduction in R&D expenses and resources [60].

Table 8 provides information on the ADMET properties of the substances predicated on factors such as water solubility, Caco2 cell permeability, skin permeability, intestinal absorption of humans, P-glycoprotein substrate, P-glycoprotein I inhibitor, Blood-Brain Barrier permeant, etc. [61]. The water-solubility properties of a substance determine how well the drug is absorbed. High water-soluble compounds have good absorption qualities and hence provide optimal drug bioavailability [62]. There were some differences in the water-soluble properties of mentioned molecules.

Table 8. ADMET properties of ketals and non-ketals.

S/N	Water solubility, Log S	Caco-2 Permeability	Blood Brain Barrier permeant	P-1 glycoprotein inhibitor	P -glycoprotein substrate	Total Clearance (ml/min/kg)	CYP450 2C9 Inhibitor	CYP450 1A2 Inhibitor
K01	-2.297	0.243	No	No	No	1.067	No	No
K02	-4.426	1.226	Yes	Yes	No	1.021	Yes	No
K03	-6.137	1.104	Yes	Yes	No	1.204	Yes	No
K04	-2.562	0.461	No	No	Yes	0.89	No	No
K05	-3.714	0.824	No	Yes	Yes	0.706	No	No
K06	-4.022	-0.095	No	No	Yes	0.346	Yes	No
K07	-2.674	0.032	No	No	Yes	0.989	No	No
K08	-4.84	1.22	No	Yes	Yes	0.937	Yes	No
K09	-4.213	1.513	No	Yes	No	0.617	Yes	No
NK01	-0.71	0.169	No	Yes	No	0.22	No	No
NK02	-3.087	-0.013	No	No	Yes	0.176	No	No
NK03	-5.46	1.223	Yes	Yes	No	0.202	Yes	No
NK04	-2.392	0.072	No	No	Yes	0.625	No	No
NK05	-3.367	0.395	No	No	Yes	0.633	No	No
NK06	-3.147	0.517	No	No	Yes	0.65	No	No
NK07	-2.101	0.334	No	No	Yes	0.673	No	No
NK08	-3.967	0.951	No	No	Yes	0.739	No	No
NK09	-3.779	1.169	No	No	Yes	0.846	No	No
Azithromycin	-2.06	0.7578	No	Yes	Yes		No	No
Nystatin	-2.892	-0.563	No	No	No	5.694	No	No
Capecitabine	-3.135	0.255	No	No	No	1.054	No	No

The molecules K01, K04, K07, NK01, NK04, and NK07 are slightly soluble in an aqueous system compared to the other molecules. While the higher water-insoluble properties of compounds K02, K03, K06, K08, K09, and NK03 refer, they are more soluble in the oil phase, such as lipids. Another important statistic is Caco-2 permeability, which evaluates a substance's flow rate through the polarized Caco-2 cell monolayers to anticipate oral medication absorption from the research conducted [63]. The Caco-2 permeability of medicine should be acceptable for effective medication. The molecules K02, NK03 & NK09 had more excellent Caco-2 permeability than the others. Only K02, K03 & NK03 compounds can produce permeant BBB among 18 derivatives simultaneously, and the ligand K03 has the larger

Total Clearance rate among all the drugs. According to this data, most drugs are not metabolized in CYP4502C9, except molecules K01, K02, K06, K08, K09 & NK03, while no drugs can inhibit the CYP450 1A2 inhibitor.

3.14. Aquatic and non-aquatic toxicity

After satisfying all of the necessary tests, therapeutic candidates may reject and withdrawn from the market because of their aquatic and non-aquatic toxicity. Because of this, medication research and discovery should need adequate safety assessments. Several indicators, including the maximum, tolerated dosage (human), oral rat acute toxicity (LD_{50}), oral rat chronic toxicity (LOAEL), hepatotoxicity, and T. pyriformis toxicity, are being used to ensure the safety of the drug and hepatotoxicity. Almost 50% of the compounds showed carcinogenicity in AMES toxicity and hepatotoxicity (Table 9). So, during the manufacturing process, they should be handled carefully in the environment, and hepatic or liver disease patients should be conscious before taking this medication due to hepatotoxicity [64].

Table 9. Aquatic and non-aquatic toxicity of ketals and non-ketals.

S/N	AMES toxicity	Hepatotoxicity	Oral Rat Chronic Toxicity (mg/kg.bw/day)	Oral Rat Acute Toxicity (LD_{50}) (mol/kg)	Max. Tolerated dose (mg/kg/day	T. Pyriformis toxicity (log ug/L)
K01	Yes	Yes	2.532	2.531	0.363	0.364
K02	No	No	2.294	1.885	0.501	0.385
K03	Yes	No	1.769	2.50	0.931	0.288
K04	No	Yes	2.353	2.386	-0.116	0.291
K05	No	Yes	2.363	2.68	0.324	0.290
K06	No	No	3.916	2.663	0.411	0.285
K07	Yes	Yes	2.10	2.395	0.578	0.269
K08	Yes	No	1.902	2.487	0.651	0.285
K09	No	No	1.633	3.17	0.711	0.285
NK01	Yes	No	3.434	1.853	0.55	0.285
NK02	Yes	No	2.842	1.814	0.470	0.382
NK03	Yes	No	1.789	1.823	0.489	0.298
NK04	No	Yes	3.677	2.145	0.859	0.285
NK05	No	Yes	3.851	2.395	0.602	0.285
NK06	No	Yes	4.537	2.745	0.821	0.285
NK07	No	Yes	3.683	2.450	0.859	0.285
NK08	Yes	No	3.644	2.592	0.288	0.285
NK09	No	No	3.124	2.475	0.389	0.285
Azithromycin	No	No	0.7761	2.5423	1.5567	0.4275
Nystatin	No	No	8.655	2.482	0.436	0.4977
Capecitabine	No	Yes	2.401	2.459	1.051	0.288

4. Conclusions

The fundamental resilience and biological activity of D-glucofuranose generated ketal and non-ketal derivatives have been explored and studied against three different diseases such as bacteria, fungus, and triple-negative breast cancer. We determined different pharmacokinetics and bioactivities of these 18 ketals and non-ketal derivatives of D-glucofuranose. We compared them to those of the conventional medication azithromycin, nystatin, and Capecitabine to determine if they have the potential to be utilized as a medication in the foreseeable.

The PASS prediction characteristics have been hypothesized to determine the biologically active compounds among these synthesis derivatives chemicals that were most

effective. PASS prediction of the ketal and non-ketal derivatives of D-glucofuranose 1–18 was 0.150<Pa<0.400 for antiviral, 0.280<Pa<0.450 for antibacterial, 0.205<Pa<0.570 for antifungal, 0.098<Pa<0.272 for antibiotic and 0.240<Pa<0.704 for antineoplastic. Based on the PASS prediction value, we have decided that the synthesized ketals and non-ketals may inhibit the best antibacterial, antifungal, and antineoplastic efficacy. With these synthetic compounds, further studies have proceeded against bacteria, fungi, and triple-negative breast cancer. Virtual screening or molecular docking, non-bonding interaction, molecular dynamics, pharmacokinetic properties, ADMET, Lipinski, etc., have been calculated. The results were correlated to Azithromycin, Nystatin, and Capecitabine values. This study indicated that all the compounds are highly stable with excellent fitting pose against targeted protein and excellent binding energy, ranging from -6.00 to -11.0 kcal/mol. Although the drugs showed hepatotoxicity and AMES toxicity in some cases, the other parameter has been satisfied as a potential drug candidate. Further *in vivo* and related studies are necessary to establish them as drug candidates.

Funding

This research was funded by the Research and Publication Cell (University of Chittagong), COVID-19 Special 2021, 124/5.

Acknowledgments

The administrative and technical support from the Department of Chemistry, University of Chittagong, is highly acknowledged.

Conflicts of Interest

The authors declare no conflict of interest.

References

1. Cao, X.; Dua, X.; Jiao, H.; An, Q.; Chen, R.; Fang, P.; Wang, J.; Yu, B. Carbohydrate-based drugs launched during 2000−2021. *Acta Pharm. Sinica B*, **2022**, https://doi.org/10.1016/j.apsb.2022.05.020.
2. Sharon, N. Carbohydrates as future anti-adhesion drugs for infectious diseases. *Biochimica Biophysica Acta* **2006**, *1760*, 527–537, https://doi.org/10.1016/j.bbagen.2005.12.008.
3. Ernst, B.; Magnani, J.L. From carbohydrate leads to glycomimetic drugs. *Nat. Rev. Drug Discovery* **2009**, *8*, 661–677, https://doi.org/10.1038/nrd2852.
4. Vimala, K.; Sivudu, K.S.; Mohan, Y.M.; Sreedhar, B.; Raju, K.M. Controlled silver nanoparticles synthesis in semi-hydrogel networks of poly(acrylamide) and carbohydrates: A rational methodology for antibacterial application. *Carbohydr. Polymers* **2009**, *75*, 463–471, https://doi.org/10.1016/j.carbpol.2008.08.009.
5. Rafin, C.; Veignie, E.; Sancholle, M.; Postel, D.; Len, C.; Villa, P.; Ronco, G. Synthesis and antifungal activity of novel bisdithiocarbamate derivatives of carbohydrates against *Fusarium oxysporum* f. sp. *Lini*. *J. Agric. Food Chem.* **2000**, *48*, 5283–5287, https://doi.org/10.1021/jf0003698.
6. Rahman, M.A.; Chakma, U.; Kumer, A.; Rahman, M.R.; Matin, M.M. Uridine-derived 4-aminophenyl 1-thioglucosides: DFT optimized FMO, ADME, and antiviral activities study. *Biointerface Res. Appl. Chem.* **2023**, *13*, 52, https://doi.org/10.33263/BRIAC131.052.
7. Peng, Q.; Peng, R.; Yuan, B.; Wang, M.; Zhao, J.; Fu, L.; *et al*. Structural basis of SARS-CoV-2 polymerase inhibition by favipiravir. *The Innovation*, **2021**, *2* 100080, https://doi.org/10.1016/j.xinn.2021.100080.
8. Dhavale, D.D.; Matin, M.M.; Sharma, T.; Sabharwal, S.G. Synthesis and evaluation of glycosidase inhibitory activity of octahydro-2H-pyrido[1,2-a]pyrimidine and octahydro-imidazo[1,2-a]pyridine bicyclic diazasugars. *Bioorg. Med. Chem.* **2004**, *12*, 4039–4044, https://doi.org/10.1016/j.bmc.2004.05.030.

9. Kerasioti, E.; Stagos, D.; Jamurtas, A.; Kiskini, A.; Koutedakis, Y.; Goutzourelas, N.; *et al.* Anti-inflammatory effects of a special carbohydrate–whey protein cake after exhaustive cycling in humans. *Food and Chem. Toxicol*. **2013**, *61*, 42–46, https://doi.org/10.1016/j.fct.2013.01.023.
10. Dhavale, D.D.; Matin, M.M. Selective sulfonylation of 4-C-hyroxymethyl-β-L-threo-pento-1,4-furanose: Synthesis of bicyclic diazasugars. *Tetrahedron*, **2004**, *60*, 4275–4281. https://doi.org/10.1016/j.tet.2004.03.034.
11. Matin, M.M.; Nath, A.R.; Saad, O.; Bhuiyan, M.M.H.; Kadir, F.A.; Hamid, S.B.A.; *et al*. Synthesis, PASS-predication and *in vitro* antimicrobial activity of benzyl 4-O-benzoyl-α-L-rhamnopyranoside derivatives. *Int. J. Mol. Sci.* **2016**, *17*, 1412, https://doi.org/10.3390/ijms17091412.
12. Matin, P.; Rahman, M.R.; Huda, D.; Bakri, M.K.B.; Uddin, J.; Yurkin, Y. *et al.* Application of synthetic acyl glucopyranosides for white-rot and brown-rot fungal decay resistance in aspen and pine wood. *BioResources* **2022**, *17*, 3025–3041, https://doi.org/10.15376/biores.17.2.3025-3041.
13. Kabir, A.K.M.S.; Matin, M.M. Regioselective monoacylation of a derivative of L-rhamnose. *J. Bangladesh Acad. Sci*. **1997**, *21*, 83–88. https://orcid.org/10.5267/j.ccl.2016.10.001
14. Young, D.C. Computational drug design: A guide for computational and medicinal chemists. John Wiley & Sons, **2009**; pp 30-80. https://doi.org/10.1002/9780470451854
15. Hohenberg, P.; Kohn, W. Inhomogeneous Electron Gas. *Phys. Rev*. **1964**, *136*, B864, https://doi.org/10.1103/PhysRev.136.B864.
16. Sharma, P.P.; Bansal, M.; Sethi, A.; Pena, L.P; Goel, V.K.; Grishina, M.; Chaturvedi, S.; Kumar, D.; Rathi, B. Computational methods directed towards drug repurposing for COVID-19: advantages and limitations. *RSC Adv*. **2021**, *11*, 36181–36198, https://doi.org/10.1039/D1RA05320E.
17. Sanaullah, A.F.M.; Matin, M.M.; Rahman, M.R.; Nayeem, S.M.A. Acyl glucopyranosides: Synthesis, PASS predication, antifungal activities, and molecular docking. *Org. Commun*. **2022**, *15*, 32–43, http://doi.org/10.25135/acg.oc.120.2201.2307
18. Vadivoo, V.S.; Mythili, C.V.; Balachander, R.; Vijayalakshmi, N.; Vijaya, P. Computational and spectral discussion of some substituted chalcone derivatives. *Biointerface Res. Appl. Chem.* **2022**, *12*, 7159–7176, https://doi.org/10.33263/BRIAC126.71597176.
19. Collin F. Chemical basis of reactive oxygen species reactivity and involvement in neurodegenerative diseases. International journal of molecular sciences. *Int. J. Mol. Sci.* **2019**, *20*, 2407, https://doi.org/10.3390/ijms20102407.
20. Tandon, H.; Chakraborty, T.; Suhag, V. A brief review on importance of DFT in drug design. *Res. Med. Engg. Sci*. **2019**, 7, 791–795, https://doi.org/10.31031/RMES.2019.07.00068 .
21. Macalino, S.J.Y.; Gosu, V.; Hong, S.; Choi, S. Role of computer-aided drug design in modern drug discovery. *Arch. Pharm. Res*. **2015**, *38*, 1686–1701, https://doi.org/10.1007/s12272-015-0640-5.
22. Fent, K.; Weston, A.A.; Caminada, D. Ecotoxicology of human pharmaceuticals. *Aquatic Toxicol*. **2006**, *76*, 122-159, https://doi.org/10.1016/j.aquatox.2005.09.009.
23. Delley, B. Time dependent density functional theory with DMol3. *J. Phys.: Condens. Matter* 2010, 22, 384208.
24. Lagunin, A.; Stepanchikova, A.; Filimonov, D.; Poroikov, V. PASS: prediction of activity spectra for biologically active substances. *Bioinformatics* **2000**, *16*, 747–748, https://doi.org/10.1093/bioinformatics/16.8.747.
25. Kumar, P.P.S.; Krishnaswamy G.; Desai, N.R.; Sreenivasa, S.; Kumar, D.B.A. Design, synthesis, PASS prediction, in-silico ADME and molecular docking studies of substituted-(Z)-3-benzylidine-5-aza-2-oxindole derivatives (Part-1). *Chem. Data Coll.* **2021**, *31*, 100617, https://doi.org/10.1016/j.cdc.2020.100617.
26. Honorio, K.M.; Moda, T.L.; Andricopulo, A.D. Pharmacokinetic properties and *in silico* ADME modeling in drug discovery. *Med. Chem.* **2013**, *9*, 163–176, https://doi.org/10.2174/1573406411309020002.
27. Ferreira, L.L.G; Andricopulo, A.D. ADMET modeling approaches in drug discovery. *Drug Discovery Today* **2019**, *24*, 1157–1165, https://doi.org/10.1016/j.drudis.2019.03.015.
28. Rahman, M.A.; Matin, M.M.; Kumer, A.; Chakma, U.; Rahman, M.R. Modified D-glucofuranoses as new black fungus protease inhibitors: Computational screening, docking, dynamics, and QSAR study. *Phys. Chem. Res.* **2022**, *10*, 195–209, https://doi.org/10.22036/pcr.2021.294078.1934.
29. Yusuf, M.; Sadiya, Ahmed, B.; Gulfishan, M. Modern perspectives of curcumin and its derivatives as promising bioactive and pharmaceutical agents. *Biointerface Res. Appl. Chem.* **2022**, *12*, 7177–7204, https://doi.org/10.33263/BRIAC126.71777204 .

30. Berman, H.M.; Westbrook, J.; Feng, Z.; Gilliland, G.; Bhat, T.N.; Weissig, H.; *et al.* The protein data bank. *Nucleic Acids Res.* **2000**, *28*, 235–42, https://doi.org/10.1093/nar/28.1.235.
31. The PyMOL Molecular Graphics System, Version 1.5.0.4. Schrödinger, LLC, New York. **2002**.
32. Greenfield, N.J.; Pietruszko, R. Two aldehyde dehydrogenases from human liver. Isolation via affinity chromatography and characterization of the isozymes. *Biochim. Biophys. Acta* **1977**, *483*, 35–45, https://doi.org/10.1016/0005-2744(77)90005-5.
33. Dallakyan, S.; Olson, A.J. Small-molecule library screening by docking with PyRx. *Methods Mol. Biol.* **2015**, *1263*, 243–250, https://doi.org/10.1007/978-1-4939-2269-7_19.
34. Accelrys Discovery Studio Modeling Environment, Release 4.0, 2013.
35. Phillips, J.C.; Hardy, D.J.; Maia, J.D.C.; Stone, J.E.; Ribeiro, J.V.; Bernardi, R.C.; *et al.* Scalable molecular dynamics on CPU and GPU architectures with NAMD. *J. Chem. Phys.* **2020**, *153*, 044130, https://doi.org/10.1063/5.0014475.
36. Skjevik, Å.A.; Madej, B.D.; Dickson, C.J.; Teigen, K.; Walker, R.C.; Gould, I.R. All-atom lipid bilayer self-assembly with the AMBER and CHARMM lipid force fields. *Chem. Commun*. **2015**, *51*, 4402–4405, https://doi.org/10.1039/C4CC09584G.
37. Sadeghi, F.; Afkhami, A.; Madrakian, T.; Ghavami, R. A new approach for simultaneous calculation of pIC50 and logP through QSAR/QSPR modeling on anthracycline derivatives: a comparable study. *J. Iran. Chem. Soc.* **2021**, *18*, 2785–2800, https://doi.org/10.1007/s13738-021-02233-9 .
38. de Oliveira, D.B.; Gaudio, A.C. BuildQSAR: a new computer program for QSAR analysis. *Quantitative Structure-Activity Relationships* **2000**, *19*, 599–601, https://doi.org/10.1002/1521-3838(200012)19:6<599::AID-QSAR599>3.0.CO;2-B
39. Mai, N.T.; Lan, N.T.; Cuong, N.T.; Tam, N.M.; Ngo, S.T.; Phung, T.T.; Dang, N.V.; Tung, N.T. Systematic Investigation of the Structure, Stability, and Spin Magnetic Moment of CrMn Clusters (M = Cu, Ag, Au, and n = 2–20) by DFT Calculations. *ACS Omega* **2021**, *6*, 20341–20350, https://doi.org/10.1021/acsomega.1c02282.
40. Lipinski, C.A.; Lombardo, F.; Dominy, B.W.; Feeney, P.J. Experimental and computational approaches to estimate solubility and permeability in drug discovery and development settings. *Adv. Drug Deliv. Rev*. **1997**, *23*, 3–25, https://doi.org/10.1016/S0169-409X(96)00423-1 .
41. Lipinski, C.A. Lead-and drug-like compounds: the rule-of-five revolution. *Drug Discov. Today Technol*. **2004**, *1*, 337–341, https://doi.org/10.1016/j.ddtec.2004.11.007.
42. Oprea, T.I.; M Davis, A.; Teague, S.J.; Leeson, P.D. Is there a difference between leads and drugs? A historical perspective. *J. Chem. Inf. Comput. Sci*. **2001**, *41*, 1308–1315, https://doi.org/10.1021/ci010366a.
43. Hanee, U.; Rahman, M.R.; Matin, M.M. Synthesis, PASS, *in silico* ADMET, and thermodynamic studies of some galactopyranoside esters. *Phys. Chem. Res.* **2021**, *9*, 591–603, https://doi.org/10.22036/pcr.2021.282956.1911.
44. Matin, M.M.; Iqbal, M.Z. Methyl 4-O-(2-chlorobenzoyl)-α-L-rhamnopyranosides: Synthesis, characterization, and thermodynamic studies. *Orbital Electron J Chem.* **2021**, *13*(1), 19–27, https://doi.org/10.17807/orbital.v13i1.1532.
45. Kumer, A.; Ahmed, B.; Sharif, M.A.; Al-Mamun, A. A theoretical study of aniline and nitrobenzene by computational overview. *Asian J. Phys. Chem. Sci.* **2017**, *4*, 1–12, https://doi.org/10.9734/AJOPACS/2017/38092 .
46. Matin, M.M.; Uzzaman, M.; Chowdhury, S.A.; Bhuiyan, M.M.H. *In vitro* antimicrobial, physicochemical, pharmacokinetics, and molecular docking studies of benzoyl uridine esters against SARS-CoV-2 main protease. *J. Biomol. Struct. Dyn.* **2022**, *40*, 3668–3680, https://doi.org/10.1080/07391102.2020.1850358.
47. Kumer, A.; Sarker, M.N.; Paul, S. The thermo physical, HOMO, LUMO, vibrational spectroscopy and QSAR study of morphonium formate and acetate ionic liquid salts using computational method. *Turk. Comput. Theor. Chem*. **2019**, *3*, 59–68, https://doi.org/10.33435/tcandtc.481878.
48. Muhammad, D.; Matin, M.M.; Miah, S.M.R.; Devi, P. Synthesis, antimicrobial, and DFT studies of some benzyl 4-O-acyl-α-L-rhamnopyranosides. *Orbital Electron J Chem.* **2021**, *13*(3), 250-258, http://dx.doi.org/10.17807/orbital.v13i3.1614
49. Neha Tiwari, N.; Uttam, G.; Priyanka; Singh, S.; Katiyar, D. In silico designing and interaction of coumarin-amino acid(s) conjugates with integrin like protein of *Cryptococcus neoformans*: Insights on antifungal drug design. *Bioint. Res. Appl. Chem.* **2021**, 11(2), 8587–8598, https://doi.org/10.33263/BRIAC0112.85878598
50. Lakshminarayanan, S.; Jeyasingh, V.; Murugesan, K.; Selvapalam, N.; Dass, G. Molecular electrostatic potential (MEP) surface analysis of chemo sensors: An extra supporting hand for strength, selectivity & non-

traditional interactions. *J. Photochem. Photobiol.* **2021**, *6*, 100022, https://doi.org/10.1016/j.jpap.2021.100022.
51. Zhang, M.; Yu, W.; Zhou, S.; Zhang, B.; Lo, E.C.M.; Xu, X.; Zhang, D. In vitro antibacterial activity of an FDA-approved H+-ATPase inhibitor, bedaquiline, against *Streptococcus mutans* in acidic milieus. *Front. Microbiol*. **2021**, *12*, 647611, https://doi.org/10.3389/fmicb.2021.647611
52. Walko, C.M.; Lindley, C. Capecitabine: a review. *Clin. Ther*. **2005**, *27*, 23–44, https://doi.org/10.1016/j.clinthera.2005.01.005.
53. Wang, K.; Zhong, H.; Li, N.; Yu, N.; Wang, Y.; Chen, L.; Sun, J. Discovery of novel anti-breast-cancer inhibitors by synergistically antagonizing microtubule polymerization and aryl hydrocarbon receptor expression. *J. Med. Chem.* **2021**, *64*(17), 12964–12977, https://doi.org/10.1021/acs.jmedchem.1c01099
54. Cao, B.-Y.; Xie, J.-F.; Sazhin, S.S. Molecular dynamics study on evaporation and condensation of n-dodecane at liquid–vapor phase equilibria. *J. Chem. Phys*. **2011**, *134*, 164309, https://doi.org/10.1063/1.3579457.
55. Kumer, A.; Chakma, U.; Matin, M.M.; Akash, S.; Chando, A.; Howlader, D. The computational screening of inhibitor for black fungus and white fungus by D-glucofuranose derivatives using *in silico* and SAR study. *Org. Commun*. **2021**, 14, 305–322, http://doi.org/10.25135/acg.oc.116.2108.2188.
56. Talarico, C.; Gervasoni, S.; Manelfi, C.; Pedretti, A.; Vistoli, G.; Beccari, A.R. Combining molecular dynamics and docking simulations to develop targeted protocols for performing optimized virtual screening campaigns on the HTRPM8 channel. *Int. J. Mol. Sci*. **2020**, *21*, 2265, https://doi.org/10.3390/ijms21072265.
57. Ouellette, R.J.; Rawn, J.D. Carbohydrates. In Organic Chemistry Study Guide: Key Concepts, Problems, and Solutions, 1st Ed, Elsevier B.V.; **2015**, 539-567, https://doi.org/10.1016/B978-0-12-801889-7.00026-1
58. Hou, T.; Wang, J.; Zhang, W.; Wang, W.; Xu, X. Recent advances in computational prediction of drug absorption and permeability in drug discovery. *Curr. Med. Chem*. **2006**, *13*, 2653–2667, https://doi.org/10.2174/092986706778201558.
59. Daoui, O.; Elkhattabi, S.; Chtita, S.; Elkhalabi, R.; Zgou, H.; Benjelloun, A.T. QSAR, molecular docking and ADMET properties *in silico* studies of novel 4,5,6,7-tetrahydrobenzo[D]-thiazol-2-Yl derivatives derived from dimedone as potent anti-tumor agents through inhibition of C-Met receptor tyrosine kinase. *Heliyon*, **2021**, *7*, e07463, https://doi.org/10.1016/j.heliyon.2021.e07463.
60. Alanazi, M.M.; Elkady, H.; Alsaif, N.A.; Obaidullah, A.J.; Alkahtani, H.M.; Alanazi, M.M. *et al*. New quinoxaline-based VEGFR-2 inhibitors: design, synthesis, and antiproliferative evaluation with in silico docking, ADMET, toxicity, and DFT studies. *RSC Adv.* **2021**, 11, 30315-30328, https://doi.org/10.1039/D1RA05925D
61. Matin, P.; Hanee, U.; Alam, M.S.; Jeong, J.E.; Matin, M.M.; Rahman, M.R.; *et al*. Novel galactopyranoside esters: Synthesis, mechanism, *in vitro* antimicrobial evaluation and molecular docking studies. *Molecules*, **2022**, *27*, 4125, https://doi.org/10.3390/molecules27134125.
62. Wuelfing, W.P.; Marrouni, A.E.; Lipert, M.P.; Daublain, P.; Kesisoglou, F.; Converso, A.; Templeton, A.C. Dose number as a tool to guide lead optimization for orally bioavailable compounds in drug discovery. *J. Med. Chem*. **2022**, *65*, 1685–1694, https://doi.org/10.1021/acs.jmedchem.1c01687 .
63. Vishvakarma, V.K.; Nand, B.; Kumar, V.; Kumari, K.; Bahadur, I.; Singh, P. Xanthene based hybrid analogues to inhibit protease of novel corona Virus: Molecular docking and ADMET studies. *Comput. Toxicol*. **2020**, *16*, 100140, https://doi.org/10.1016/j.comtox.2020.100140.
64. Wang, Y.; Xing, J.; Xu, Y.; Zhou, N.; Peng, J.; Xiong, Z.; *et al*. *In silico* ADME/T modelling for rational drug design. *Q. Rev. Biophys*. **2015**, *48*, 488–515, https://doi.org/10.1017/S0033583515000190.